This is the author's version of an article that has been published in this journal. Changes were made to this version by the publisher prior to publication.
The final version of record is available at http://dx.doi.org/10.1109/TPEL.2021.3063499

IEEE POWER ELECTRONICS REGULAR PAPER/LETTER/CORRESPONDENCE

An Investigation into High Voltage Spiral Generators Utilizing Thyristor Input Switches

Jiaqi Yan, Susan Parker, and Simon Bland, *IEEE member*

***Abstract*— High voltage nanosecond pulses are widely used in scientific research, but their wider adoption in industry requires compact, cost effective and easy to use generators to be developed. This paper presents modelling and experimental investigations into one method of producing such pulses – a spiral generator with a solid-state, thyristor-based input switch. It includes how the pulses are formed within the spiral, why a high speed input switch is required, how the geometry of the spiral dictates its output characteristics, and the effects of different loads. Using thyristors, often connected in series to increase the operating voltage of the spiral, enables the spiral generators to have low jitter, high repetition rate, and long lifetime. Modelling of the circuit used a combination of telegraph equations to account for the wave propagation along the spiral and a lumped circuit exchanging charge between the spiral, the input switch, and the load. The model is verified by detailed experimental results with the relative error being < 10% in most cases. The output voltage pulse was often observed to have an initial peak of much lower magnitude than the subsequent peak(s) – which can only be fully explained by considering wave propagation effects. Lower input switch inductance, shorter switching time, larger mean diameter of the spiral, and increasing the width of the copper tape that makes up the spiral can all increase the voltage multiplication efficiency. Though increasing the number of turns that make up the spiral can increase the output voltage, it can also lower the multiplication efficiency. By understanding the effects of different geometries the spiral can be optimized to drive different loads - three applications of such spiral generators are then presented: pulses with 10 kV amplitude and 10 kHz repetition rate for driving DBD plasma, pulses with amplitude of 10 kV and 10 kV/ns rising rate for triggering of advanced solid state switches, and pulses with -50 kV amplitude and 50 ns rising time for triggering high current gas switches through field distortion.[1]**

***Index Terms*—spiral generator, nanosecond pulses, telegraph equations, series-connected thyristor module, pulse forming process**

I. Introduction

PULSED power systems are becoming more popular in scientific and industrial applications, especially as advances enable them to become more compact and convenient to utilize. High voltage pulses are, for instance, used to drive low temperature plasmas [1], [2], remove water contaminants [3], trigger high power switches [4], and produce X-ray radiography sources [5]. Short duration (10s of ns) pulses are especially sought after as in this case the efficiency of particle activity is significantly increased in low temperature plasmas [6], the triggering of high power switches has an equivalently small jitter, and radiographs of even high speed objects can be time resolved. There are several methods commonly used to make such pulses including Marx generators [7], [8], pulse transformers [9], Tesla transformers [10] and Linear Transformer Drivers (LTDs) [11]. Great efforts are put into developing such devices and increasing their reliability.

This paper presents an in-depth investigation into a different method of producing high voltage, short duration pulses, the spiral generator, which was first introduced in 1964 by Fitch and Howell [12]. Spiral generators are a type of Vector Inversion Generator (VIG) and typically consist of a copper tape stripline wrapped around itself with an extra layer of insulation (Fig. 1). In contrast to Marx or LTD generators, the spiral generator only has two or three parts: a low inductance input switch, a spiral stripline, and - if needed - an output pulse sharpening gap. The energy of the generator is capacitively stored in the stripline itself. With one side of the stripline charged to u_0 by a DC power supply, closure of the input switch results in an output pulse of amplitude of u_{out}=-$2\varepsilon_{ff}Nu_0$ on the load, where ε_{ff} is the voltage multiplication efficiency and N is the number of turns of the spiral. It is a simple and cost effective way of producing voltage pulses of 10s to 100s kV amplitude from low initial charging voltages. Providing no magnetically permeable material is used, the voltage multiplication ratio remains unchanged when adjusting charging voltage. Comparing to a Tesla transformer, it is much simpler, and it is not necessary to meet the criteria of resonance between primary and secondary circuit.

However, despite their simplicity, spiral generators have found relatively few uses, and most of these are restricted to within pulsed power based science. In the 1970s-2000s, several companies and labs produced spiral generators to act as triggers for high-current spark gap switches [13]. From 2003 to 2009, Rose *et al*. at Radiance Technologies, Inc. conducted detailed experimental studies, including failure characteristics and design criteria [14]-[18]. In 2006, Shkuratov *et al*. at Loki Inc. utilized spiral generators as the power-conditioning stage in an explosive ultracompact high-voltage nanosecond pulse-generating system [19], [20].

Jiaqi Yan is with the Plasma Physics Group, Blackett Laboratory, Imperial College London, London, SW7 2BW, United Kingdom, and the State Key Laboratory of Electrical Insulation and Power Equipment, Xi'an Jiaotong University, Xi'an, 710049, China. (E-mail: yanjqxjtu@foxmail.com)

Susan Parker and Simon Bland are with the Plasma Physics Group, Blackett Laboratory, Imperial College London, London, SW7 2BW, United Kingdom. (E-mail: s.parker@imperial.ac.uk; sn.bland@imperial.ac.uk)

This work is supported by First Light Fusion Ltd and the U.S. Department of Energy under Cooperative Agreement Nos. DE-NA0003764 and DE-SC0018088. Corresponding author: Simon Bland.

Copyright (c) 2021 IEEE. Personal use is permitted. For any other purposes, permission must be obtained from the IEEE by emailing pubs-permissions@ieee.org.

This is the author's version of an article that has been published in this journal. Changes were made to this version by the publisher prior to publication.
The final version of record is available at http://dx.doi.org/10.1109/TPEL.2021.3063499

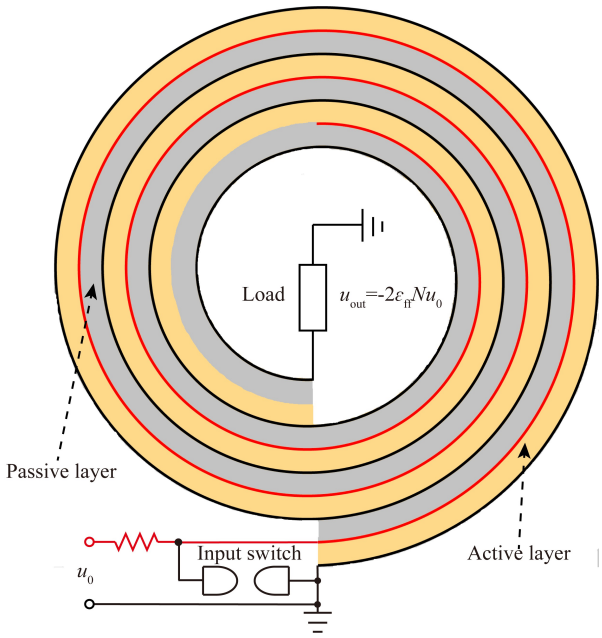


Fig. 1. Schematic of a spiral generator. Red and black represent conducting foils/tape, orange the insulation of the 'active' layer and grey the insulation of the 'passive' layer. The red wire indicates the charged conductor. Generally, 10 or more turns are used. Conducting tape is usually made of copper and the insulation of Mylar.

Sheftman *et al*. at Technion [21] and Pal'chikov *et al*. at Russian Academy of Sciences [22] have used large spiral generators as the basis for pulsed X-ray imaging apparatus.

According to references and our experiences, there are three main reasons for the lack of uptake in the use of spiral generators. Firstly, modelling and analysis of the underlying physics has been sparse. Despite the simplicity of the spiral generator structure, the pulse forming process is complicated due to the simultaneous existence of wave propagation within the spiral and lumped circuit characteristics outside. Hence, designing for certain applications relied on a combination of phenomenological arguments and empirical testing of many prototypes. Secondly, it has become difficult to find input switches with a sufficiently fast changing rate of impedance and sufficiently low inductance to get efficient voltage multiplication in a spiral generator - 100s A to 10s kA must be switched in a few ns. Krytrons, which were used in the popular 'PT55' generators, are no longer manufactured [13]. Miniature triggered spark gaps have often been used to perform this role, however, they can only operate in a single shot mode or at a low repetition rate (and also require a fast pulse of several kV to maintain low jitter - a complication increasing the complexity of the circuit). Thirdly, the influence of the geometric parameters of the spiral (its diameter, stripline width etc) on its output, and how different types of load can affect its output, have seldom been experimentally studied.

In this paper we hope to address these deficiencies. We have developed 'all solid-state' high voltage spiral generators using ultra-fast thyristor based input switches, typically in a series connected architecture, to enable operation at relatively high voltages replacing the traditional Krytrons or spark gaps. We have also explored in detail how a spiral generator can be modelled. Following Pal'chikov's work [23], we employed telegraph equations to study how voltage waves travel inside the spiral. Additionally, we introduced more realistic parts to our model including resistive losses inside the spiral, the turn-on rate of the input switch, and the exchange of charge between the spiral and the input switch and load. We also modified the calculation of output voltage from the original work by Pal'chikov to obtain more relevant results. Our model is verified against experiments, including the first comprehensive measurements of how the voltage waves travel and interact inside the spiral; and the effects of different input switch inductance, load inductance, load capacitance and load resistance. For many loads, particularly those with small capacitance, our simulations were in very good agreement with the experimental results; for other loads the simulations at least repeated the observed trends in output voltage. Finally, we have explored the effects of the geometry of the spiral – its number of turns, diameter, and the width of the copper tape employed making the spiral - on the output voltage waveform. Again, experimental results are compared to modelling, enabling us to draw better conclusions on how these factors affect the voltage multiplication efficiency.

The structure of the remainder of this paper is as follows. In Section II we describe the general operation principle of the spiral generator and modelling efforts prior to this paper. In Section III we discuss how we have modelled the spiral generator. Section IV describes our experimental work to compare to the model's predictions, providing detailed measurements of the effects of input switch impedance, the spiral geometry, and different loads. Output pulses for three different applications are then presented - to drive a dielectric barrier discharge; to drive a new type of high current semiconductor switch that requires extreme rates of rise of voltage (>2 kV/ns); and to trigger a high current spark gap through field distortion. Finally, section V presents our conclusions and plans for future work.

II. Theoretical Analysis of Spiral Generator

A. General operation principle of spiral generators

As shown in Fig. 1, a spiral generator consists of an input switch, a stripline that is tightly rolled up into a spiral with an additional layer of insulation employed between the layers, and a load. A pulse sharpening gap can be inserted just prior to the load if needed. The geometry of the stripline effectively forms two transmission lines or 'layers' with a shared middle conductor that is charged to u_0 by the DC power supply. The charged conductor is connected by the input switch to the outer grounded conductor - this forms what is typically called the 'active layer' of the spiral either side of the orange-colored insulator in Fig. 1. The other layer, between the charged conductor and the next inner grounded conductor, is called the passive layer (either side of the grey insulator in Fig. 1). At inner end of the spiral, the charged conductor is left open

Copyright (c) 2021 IEEE. Personal use is permitted. For any other purposes, permission must be obtained from the IEEE by emailing pubs-permissions@ieee.org.

This is the author's version of an article that has been published in this journal. Changes were made to this version by the publisher prior to publication.
The final version of record is available at http://dx.doi.org/10.1109/TPEL.2021.3063499

whilst the grounded conductor is connected to the load directly or through the pulse sharpening gap.

The first attempt at analyzing the behavior of the spiral generator was a phenomenological approach in the original Fitch and Howell paper [12]. With the input switch open the electric field vectors in the active and passive layers have equal magnitudes and opposite directions. Once the switch closes, the passive layer is assumed unaffected as voltage wave propagates along the active layer. This wave is reflected by the open connection at the other end of the charged conductor, swapping the direction of electric field vector in the active layer so the vectors in each layer are now aligned. As the wave reaches the input switch, the output voltage reaches a peak (u_{out}=-2$\varepsilon_{ff}Nu_0$), and the risetime of the output voltage, t_r=2$N\pi D/c_{eff}$, is the time taken for the voltage wave to travel back and forth through the spiral, where D is the mean diameter of the winding, and c_{eff} is the wave propagation velocity in the spiral. Whilst the risetime of the first voltage pulse seen in experiments usually agrees well with this estimate, the model does not predict the voltage multiplication efficiency or the complex oscillatory structure of the output after the first pulse. Indeed, subsequent peaks in voltage can be much higher and are potentially more useful in application.

B. Series-connected thyristor modules as input switches

Simple calculations based on the capacitance and inductance of the spiral generator suggest that with charging voltages of a few kV, the input switch must be capable of handling peak currents of 100s to 1000s of Amps, with rising edges of 10s A/ns to ~100 A/ns. Further, empirical results and previous modelling suggest that the voltage multiplication efficiency of a spiral generator is greatly influenced by inductance and on-state impedance of the input switch [12], [24]. As stated in Section I, miniature triggered spark gaps have therefore often been used as input switches. To achieve reliable, low jitter performance, such spark gaps require their own high voltage (few kV), short risetime trigger pulses - further complicating their use. The lifetime and repetition rate of these spark gaps is also limited.

To overcome these drawbacks, use of a solid-state input switch would be highly desirable. However, the combination of high current, fast risetimes, several kV charging voltages and low overall inductance are difficult to obtain. Our initial investigations explored several different types and topologies (serial and parallel) of solid-state input switches, however most proved unsuitable, with the spiral generator not showing any large voltage multiplication, and often major damage occurring to the switch itself. Following a presentation at the 2019 IEEE PPPS conference [25], we found that the ultra-fast SP205-01 thyristors, a.k.a. 'Solidtrons', recently developed by Silicon Power Corporation [26], [27], could be utilized. These have a unique internal structure with much smaller internal cell sizes that are far more densely packed, giving significant improvements in current uniformity within the device (so helping prevent hot spot formation). Each is rated to 65 A/ns with a peak anode current of 2.7 kA. Further, whilst these thyristors each has a hold-off voltage of 1.5 kV, they were designed to be readily stacked in series and triggered together, immediately enabling higher voltage use.

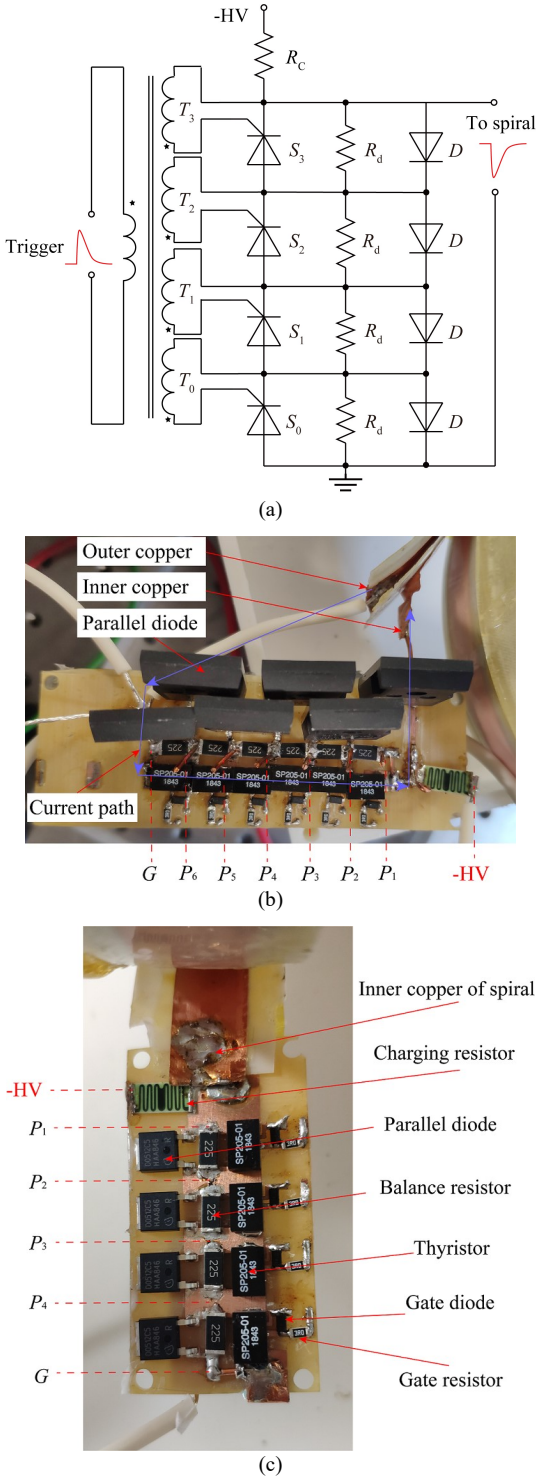


Fig. 2 Series-connected thyristor modules as input switch. (a) electrical circuit of 4 thyristors in series, the gate resistors and gate diodes are not drawn in the figure, and the 6 thyristors module has a similar structure; (b) picture of module (i) - 6 thyristors in series, the current path is marked by the blue line; (c) picture of module (ii) - 4 thyristors in series, the current returns through the copper printed on the back of PCB.

Copyright (c) 2021 IEEE. Personal use is permitted. For any other purposes, permission must be obtained from the IEEE by emailing pubs-permissions@ieee.org.

This is the author's version of an article that has been published in this journal. Changes were made to this version by the publisher prior to publication.
The final version of record is available at http://dx.doi.org/10.1109/TPEL.2021.3063499

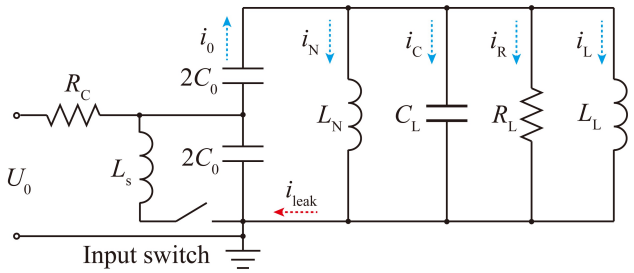


Fig. 3 Equivalent circuit of a spiral generator used to consider the charge exchange during voltage multiplication process. U_0 is the charging voltage and R_C the charging resistor (this is large enough that it plays no part in the discharge of the spiral).

Fig. 2 shows two kinds of series-connected thyristor modules developed with the SP205 Solidtrons. Module (i), shown in Fig. 2(b), was the first module constructed for the project. It uses 6 thyristors in series and has a relatively large inductance of 40-50 nH due to long current path dominated by trailing leads connecting it to the spiral. The more optimized module (ii) shown in Fig. 2(c) was developed to study the effects of input switch inductance. Here only 4 thyristors are used in series, and the current returns through the copper printed on the back of PCB. This along with close coupling to the spiral reduced its inductance to ~10 nH. In both circuits, resistors R_d (2 MΩ/1 W, size of 2512) and SiC Schottky diodes D (C5D10170H/1.7 kV for module (i) and IDM05G120C5/1.2 kV for module (ii)) are used to guarantee the voltage sharing among thyristors to be even. The charging resistor and gate resistor are 100 kΩ/2 W and 3 Ω/0.25 W, respectively. A diode (BAV16W/1N4148W) is connected between the gate and the emitter of the thyristor. All components are surface mounted to make the circuit as compact as possible. Both modules utilize magnetic coils made of NiZn Ferrite (not shown in the figure) for each thyristor to isolate the floating high voltage and transfer the trigger pulse. P_1-P_6 are the voltage measuring points, and G is the ground. By measuring the voltage between these points to the ground, the voltage on each thyristor can be obtained.

Full details of the experimental setup used to test the spiral generators will be addressed in Section IV. Using either module (i) or module (ii) as the input switch enabled the spiral generator to produce output pulses with amplitude of ~50 kV.

C. Previous efforts to model the operation of spiral generators

There have been several previous attempts to model the output of the spiral generator. In 1980, Rühl and Herziger [24] utilized Laplace transforms and a simple equivalent (lumped) circuit model to explore the dependence of the output on resistive loses in the layers, the risetime of the input switch, and the impedance of the load. This enabled some predictions of the shape of the voltage pulse, but the paper did not consider the discharge of the passive layer (and lacked comparison to experimental results). In 2007 Bichenkov *et al.* [28] made crucial improvements to the Rühl and Herziger model, enabling the discharge of the passive layer to be considered, and then modelled the spiral as a variant of a Tesla Transformer. For a relatively small number of turns (N=10) the latter model especially provided a good prediction of a spiral generator's output as it oscillated back and forth; however, neither model matched the output of a spiral generator with a large number of turns well beyond the initial rise of the first voltage pulse.

In 2012, Pal'chikov *et al.* [23] took a very different approach to modelling of the spiral. Realizing that with an increasing number of turns, the complex interaction of the voltage waves between the layers would make a simple lumped circuit approach untenable, they instead sought to simulate the waves within the spiral in one dimension via telegraph equations. This approach enabled predictions of the spiral generator output with a different number of turns and when utilizing different arrangements of switching/charging the different layers, such as a Belkin-Zharkova transformer. In 2019, they further extended boundary conditions to cases considering additional inner and outer turns [22]. However, neither paper explored in depth how the model behaved with different input switch characteristics or when coupled to different load impedances. As in most previous studies, the model was formulated for and compared to experiments utilizing a magnetic core in the spiral generator to increase the voltage multiplication efficiency; often the use of a core can be detrimental to other generator characteristics. Further, the simulation results were only qualitatively compared to the experimental results.

III. Modelling of the Spiral Generator

A. Equivalent circuit and telegraph equations

Based on the previous studies described above, we decided to model the spiral generator through two methods coupled via the input and output of the stripline that formed the spiral. Telegraph equations, similar to those used by Pal'chikov, allowed for wave propagation in the stripline. The charge exchange between the stripline and input switch/load were incorporated through an equivalent circuit. Critically this enabled the inductance/resistance of the input switch, along with the characteristics of the load, to alter wave propagation within the spiral, which was usually ignored in other models.

The equivalent circuit is shown in Fig. 3. This included the input switch (including inductance L_s), the combination of inductance L_L, resistance R_L, and capacitance C_L, that make up the load, along with the output capacitance C_0 of the spiral, and the inductance of its turns, L_N. Many previous papers present contradictory formulae for C_0 and especially L_N, making comparisons between models unnecessarily difficult. Here we use calculated C_0 from [24]:

$$C_0 = \frac{\varepsilon_r \varepsilon_0 \pi D w}{2Nt} \tag{1}$$

where w is the width of the copper tape, t_i is the thickness of single insulation layer, and ε_0 and ε_r are the vacuum and relative permittivity, respectively. We note that there are two layers of the spiral, i.e. the active layer and the passive layer.

Copyright (c) 2021 IEEE. Personal use is permitted. For any other purposes, permission must be obtained from the IEEE by emailing pubs-permissions@ieee.org.

This is the author's version of an article that has been published in this journal. Changes were made to this version by the publisher prior to publication.
The final version of record is available at http://dx.doi.org/10.1109/TPEL.2021.3063499

When considering the total output capacitance of the spiral, these two layers are regarded to be connected in series, and the total value is C_0. Thus, the capacitance of each layer is two times the output capacitance, i.e. $2C_0$, as shown in the equivalent circuit. L_N is calculated from the formula for a multi-turn winding coil [29]:

$$L_N = K' \frac{\mu_r \mu_0 \pi D^2 N^2}{2w} \tag{2}$$

K' is determined by the geometric parameters and in our case, it is usually 0.159. μ_0 and μ_r are the vacuum and relative permeability, respectively. According to the structure of the spiral generator, L_N can be easily measured by the LCR meter while C_0 only "exists" in the transition of pulse forming process and is usually calculated from the input capacitance C_{in}, which can be measured at the input terminal and has the relationship of $C_{in}=2N^2C_0$.

Based on the equivalent circuit, the circulating current i_N flowing through inductance of the spiral can be calculated from (3), where i_0, i_L, i_C and i_R are the current flowing through the capacitance of the spiral, the inductance, the capacitance and the resistance of the load, respectively, which can be calculated from (4)-(7). When the output terminal is open ended, $i_{leak} \approx i_N$.

$$i_N = i_{leak} - i_0 - i_R - i_L - i_C \tag{3}$$

$$i_0 = \frac{1}{2N^2} \frac{du_s}{dt} \tag{4}$$

$$i_R = \frac{l}{2N^2 c C_0 R_L} u_s \tag{5}$$

$$\frac{N^2 L_L}{L_N} \frac{di_L}{dt} = \frac{\omega_0^2}{2} u_s \tag{6}$$

$$i_C = \frac{C_L}{2N^2 C_0} \frac{du_s}{dt} \tag{7}$$

Once the input switch closes, both the current leaking through turns of the spiral, i_{leak}, and the current driven through the load, i_R, i_L and i_C, flow along the copper tape shown in black color in Fig. 1, from the ground to the output terminal. The charge is supplied through current i_N by the distributed capacitance formed by the long stripline. For applications like pulsed X-ray generation and triggering of high voltage gas switches, the load can be regarded as a very small stray capacitance. However, the load can also be resistive, inductive, and even of mixed type in some conditions, which our model allows.

The Telegraph equations used to describe wave propagation in both the active and passive layers were based on the those described by Pal'chikov [23]. Here the equations for wave propagation were simplified by transforming real values of position X, time T, voltage U and current I into a system of dimensionless variables "x, t, u and i" where:

$$X = lx\,,\ T = \frac{l}{c_{eff}} t\,,\ U = u_0 u\,,\ I = c_{eff} C' u_0 i \tag{8}$$

here $l=N\pi D$ is the total length of the unrolled stripline, and $C'=2N^2C_0/l$ is the capacitance of the unit length. $x = 0$ is the input of the generator, and $x = 1$ is the output end; $t = 0$ is when the switch is closed, and $t = 1$ is the time for a wave to propagate from one terminal of the spiral to the other; $u = 0$ is zero voltage, $u = 1$ is the input voltage; $i = 0$ is zero current, and $i = 1$ is the average charge changing in the single turn when the voltage on active layer is completely discharged from u_0 to 0.

Telegraph equations describing the spiral can be written as sets of (9) and (10), where u_a, i_a, u_p and i_p are the normalized voltage and current of active and passive layers, respectively.

$$\begin{cases} \dfrac{\partial u_a}{\partial x} = -\dfrac{\partial i_a}{\partial t} - \dfrac{2c_{eff} N^2 R_0 C_0}{l} i_a \\ \dfrac{\partial i_a}{\partial x} = -\dfrac{\partial u_a}{\partial t} - N i_{leak} \end{cases} \tag{9}$$

$$\begin{cases} \dfrac{\partial u_p}{\partial x} = -\dfrac{\partial i_p}{\partial t} - \dfrac{2c_{eff} N^2 R_0 C_0}{l} i_p \\ \dfrac{\partial i_p}{\partial x} = -\dfrac{\partial u_p}{\partial t} - N i_{leak} \end{cases} \tag{10}$$

We assume that any leakage current due to the conductivity of the stripline, i_{leak}, flowing through turns is constant along the whole stripline, hence:

$$\frac{\partial i_{leak}}{\partial x} = 0 \tag{11}$$

Diverging from Pal'chikov's work, we wish to explore the effects of resistive losses in the spiral and so calculate the total resistance of the spiral R_0 from eqn (12), where ρ is the resistivity of copper tape with the value of 1.74×10^{-8} Ω·m.

$$R_0 = \frac{\rho l}{S} = \frac{\rho l}{w\Delta} \tag{12}$$

$$\Delta = \sqrt{\frac{2\rho}{\omega \mu_0 \mu_r}} \tag{13}$$

Here Δ is the skin depth of the conducting layer. In the case of spiral generators utilized in our research, the frequency of oscillations is typically a few MHz, and the skin depth approximately equals to the thickness of the conducting tape, 30 μm, used to construct the spiral generator.

In a further difference to Palchikov's paper, we calculate the output voltage of the spiral generator u_s by integrating the sum of the voltage on active layer u_a and the voltage on passive layer u_p along the total length of the spiral stripline, rather than over the number of turns N:

$$u_s = l \int_0^1 (u_a + u_p) dx \tag{14}$$

B. Boundary conditions and initial conditions

To obtain the solution of the telegraph equations, proper initial conditions and boundary conditions need to be determined. Usually, the charging voltage is negative, hence we can write initial conditions as:

$$u_a(x,0) = -1 \tag{15}$$

$$u_p(x,0) = 1 \tag{16}$$

$$i_a(x,0) = i_p(x,0) = 0 \tag{17}$$

Copyright (c) 2021 IEEE. Personal use is permitted. For any other purposes, permission must be obtained from the IEEE by emailing pubs-permissions@ieee.org.

This is the author's version of an article that has been published in this journal. Changes were made to this version by the publisher prior to publication.
The final version of record is available at http://dx.doi.org/10.1109/TPEL.2021.3063499

There are two borders to the model. For the input terminal, the conditions address the influence of the inductance and switching impedance of input switch, which determines the relationship between i_N and u_s, i_a and u_a, and i_p and u_p. These currents are inductively coupled by the magnetic flux, and coefficients k_{ap}, k_{sa} and k_{sp} are used to describe their mutual influence. Because of the close contact between active and passive layers, k_{ap} is close to unity, and $k_{sa}\approx k_{sp}\ll 1$. In the model, we select $k_{ap}=0.9$ and $k_{sa}=k_{sp}=0.1$, as shown in Table I. Thus, the boundary conditions at the input are

$$N^2\frac{di_N}{dt}+k_{sa}Nn\frac{di_{0a}}{dt}-k_{sp}N(n+1)\frac{di_{0p}}{dt}=\frac{\omega_0^2}{2}u_s \tag{18}$$

$$-(L_z+n^2)\frac{di_{0a}}{dt}+(L_z+k_{ap}n(n+1))\frac{di_{0p}}{dt}-k_{sa}Nn\frac{di_N}{dt}+\frac{R_s l}{L_0 c}i_{0a}=\frac{\omega_0^2}{2}u_{0a} \tag{19}$$

$$(L_z+k_{ap}n(n+1))\frac{di_{0a}}{dt}-(L_z+(n+1)^2)\frac{di_{0p}}{dt}+k_{sp}N(n+1)\frac{di_N}{dt}+\frac{R_s l}{L_0 c}i_{0p}=\frac{\omega_0^2}{2}u_{0p} \tag{20}$$

Here n is the number of additional outer turns of the active layer, and in our experimental setup it always equals to zero. To include the speed of the input switch into our model we made R_s time dependent using the stepwise function shown in (21). R_{open} is the open impedance of the switch, typically > 1 GΩ, whilst the on-state of the input switch is usually smaller than 100 mΩ. The rate at which the switch transition between the 2 values is the drop rate, $f_{step}(t)$. Other parameters in the boundary conditions include ω_0, which is the normalized oscillation frequency of the circuit shown in Fig. 3, whilst L_z is the ratio of the switch inductance to the inductance of the single turn of the spiral:

$$R_s=R_{open}f_{step}(t) \tag{21}$$

$$\omega_0=\frac{1}{\sqrt{L_N C_0}}\frac{l}{c_{eff}} \tag{22}$$

$$L_z=\frac{L_s}{L_N/N^2} \tag{23}$$

For the output terminal, because the charged copper tape is left open ended, the wave current at this point should remain zero during the whole operation of the spiral i.e.:

$$i_a(1,t)=i_p(1,t)=0 \tag{24}$$

The telegraph equations and the coupling of the spiral to the equivalent circuit were solved through finite element analysis in the Partial Differential Equation (PDE) module of COMSOL. A list of the main parameters used by/calculated for the model are shown in Table I. The geometrical parameters are based on a spiral generator developed in this project to trigger a high voltage spark gap switch; the details can be found in [30]. The output inductance and capacitance are calculated from equations (1) and (2). The electromagnetic wave speed is calculated from equation (25), where the relative permittivity $\varepsilon_r\approx 3$ and the relative permeability $\mu_r\approx 1$ of Mylar. T_0 is the time required for the wave to propagate from one terminal to the other of the spiral, and the inductance of input switch L_s is estimated from the length of the electrical circuit of the input switch.

$$c_{eff}=c/\sqrt{\varepsilon_r\mu_r} \tag{25}$$

TABLE I
TYPICAL PARAMETERS USED IN CALCULATION OF THE MODEL AND THE EXPERIMENTS

Factor	Symbol	Values
Number of turns	N	24
Length of the spiral	l	9.05 m
Copper width	w	12 mm
Mean diameter of the winding	D	120 mm
Thickness of the winding	t_h	20 mm
Thickness of copper	t	30 μm
Thickness of single insulation layer	t_i	250 μm
Wave speed in the stripline	c_{eff}	**1.73×10^8 m/s**
Characteristic time	T_0	**52.25 ns**
Output inductance	L_N	**111.77 μH**
Output capacitance	C_0	**20 pF**
Inductance of input switch	L_s	**10 nH**
Coupling coefficient	k_{sa}, k_{sp}	0.1
Coupling coefficient	k_{ap}	0.9

In summary, our model presents a number of improvements over those previously employed – it can account not only for wave propagation within the stripline as in [23] but also for the characteristics of the input switch and load. It incorporates resistive losses as in [24] and corrects/modifies calculations of the output voltage u_s compared to [23]. Together these improvements enable detailed, direct comparison with a wide range of experimental data to help validate our model and explore its drawbacks.

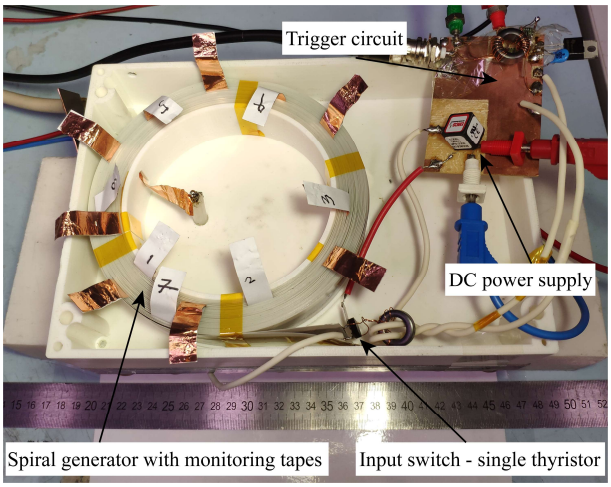
IV. Experimental Testing and Validation

A. Experimental setup

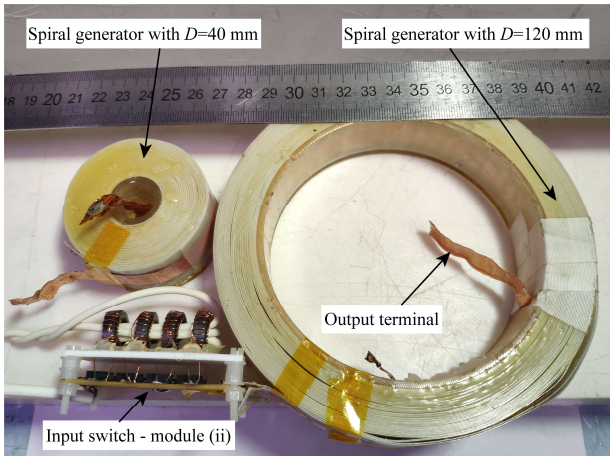
Examples of different spirals, along with their input switches, are shown in Fig. 4. In most cases, the spiral winding employed for our experimental tests used 12 mm wide, 30 μm thick copper tape, laminated onto 25 mm wide Mylar strip, 250 μm thick. An SLA printed former of 100 mm diameter was used to support the windings, which were wound under constant tension. 24 windings were made, then the spiral was impregnated with high voltage epoxy using a vacuum oven and then dried. The outer diameter of a finished spiral was ~140 mm and the DC breakdown voltage across the layers of the stripline in the spiral was greater than 10 kV. To

Copyright (c) 2021 IEEE. Personal use is permitted. For any other purposes, permission must be obtained from the IEEE by emailing pubs-permissions@ieee.org.

This is the author's version of an article that has been published in this journal. Changes were made to this version by the publisher prior to publication.
The final version of record is available at http://dx.doi.org/10.1109/TPEL.2021.3063499



(a)

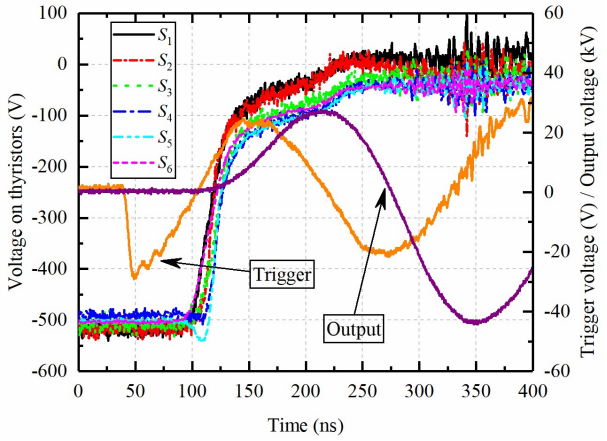


(b)

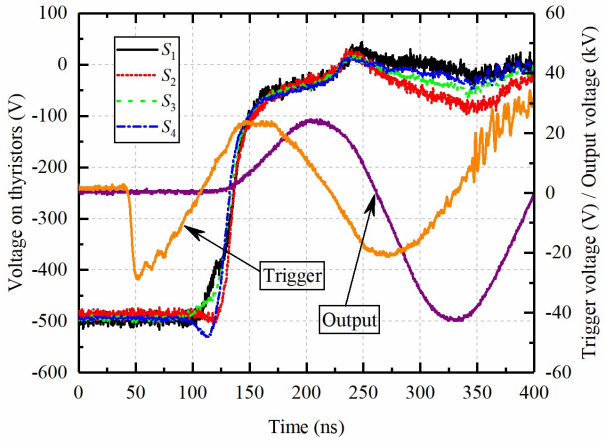
Fig. 4. Photographs of different spiral generators used in our experimental tests (a) setup of the spiral generator with monitoring tapes for studying pulse forming process; (b) spiral generators with D=40 mm and D=120 mm, and the latter one using the low inductance 4 Thyristor module (ii) as the input switch. For both spirals, N=24 and w=12 mm.

explore wave propagation, one version of the spiral generator was constructed with monitoring tabs every third turn on the active and passive layers shown in Fig. 4(a). When studying the effects of spiral geometry, the mean diameter of winding, the width of copper tape and the number of turns were all adjusted.

As stated in Section IIB, two series-connected thyristor modules were used as input switches to the spirals. Module (i) had a relatively high inductance ~40-50 nH due to long connection leads and a widely spaced design. Module (ii) was significantly more optimized by using the current returning structure with an inductance of ~10 nH. Charging voltages up to ~5 kV were employed in our tests, along with loads employing resistors from 100 Ω to 100 MΩ, capacitors from 5 to 300 pF, and inductors from 1 μH to 1 mH. A Tektronix P6015a probe rated at 40 kV with a bandwidth of 75 MHz measured the output of the spiral generator across the load. The probe itself had an input capacitance of 3.3 pF and an



(a)



(b)

Fig. 5. Switching voltage waveforms on each thyristor when the spiral generator operates. (a) 6 thyristors in series; and (b) 4 thyristors in series. The voltage on each thyristor is ~500 V. The output terminal of the spiral is open-ended.

input impedance of 100 MΩ. Although the output voltage from the spiral could reach above the rated value of the probe, measurements were still possible due to the very short timescale of the output preventing any breakdown. In our case, the output pulse from the spiral had a highest amplitude of ~50 kV and a pulse width of ~100 ns, while the certified voltage of the Tektronix P6015a probe should be <40 kV with the pulse width <1 ms according to the datasheet. Note that to make the comparison between simulation and experiment clearer, many figures adopt normalized voltage, that is, the unit is u_0.

Typical switching waveforms of the 4 and 6 thyristors modules are shown Fig. 5. In these tests the output terminal of the spiral is open-ended. The voltage between the emitter of each thyristor and the ground was measured, shown as the points of P_1 to P_6 in Fig. 2(b) and the points of P_1 to P_4 in Fig. 2(c), and the voltage on each thyristor then calculated. As can be seen from Fig. 5, the dropping/switching process of each thyristor consists of two parts – the initial state and the on state. The thyristor voltage decreases rapidly to about 20% of the charging voltage in the initial state during ~50 ns, which approximately equals to the characteristic time T_0 of the

Copyright (c) 2021 IEEE. Personal use is permitted. For any other purposes, permission must be obtained from the IEEE by emailing pubs-permissions@ieee.org.

This is the author's version of an article that has been published in this journal. Changes were made to this version by the publisher prior to publication.
The final version of record is available at http://dx.doi.org/10.1109/TPEL.2021.3063499

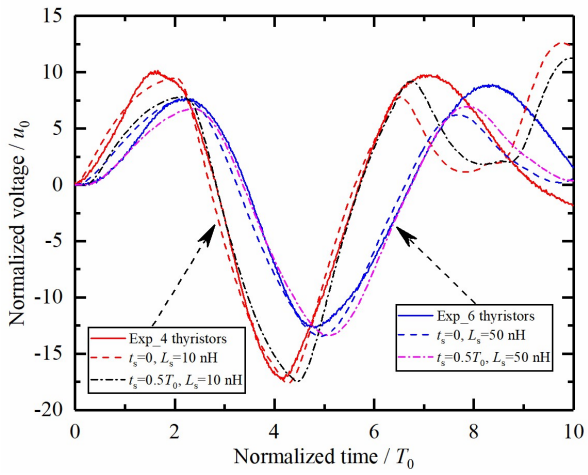


Fig. 6. Comparison between experiment and simulation for spiral generators driving electric field distortion in a Kovalchuk ball switch. Two different experiments were performed, and the same setup of the spiral is used: one using the 6 thyristors module (i) (high inductance) as input switch and a charging voltage -4.5 kV, and the other using 4 thyristors module (ii) (optimized) as input switch and -3.6 kV. In the models, the Kovalchuk ball switch and voltage probe combined were represented as a 10 pF capacitive load. The models with resistive loss assume a 0.42 Ω resistance in the spiral (calculated from the resistivity of the copper foil). T_0=52.25 ns.

voltage wave traveling from the input terminal to the output of the spiral. In the on state, each thyristor's voltage then slowly changes and approaches zero just after the peak of the output voltage pulse from the spiral. These characteristics are similar to those recorded by Waldron [26] who explored the use of arrays of the SP205-01 thyristors as an Ignitron replacement.

A detailed examination of the voltages in the 4 thyristors circuit shown in Fig. 5(b) indicates that S_1 and S_3 turn on faster to the initial state than S_2 and S_4, and the latter two thyristors suffer a small overvoltage. This inconsistency is likely caused by the slightly different trigger conditions, including the windings of trigger coils, the positions of thyristors, and the turn-on delay of thyristors, etc. The waveforms of the fast dropping edge then rapidly become consistent with each other, though after the zero-crossing point, the residual voltage on each thyristor varies slightly. Note that the residual voltage on each transistor is only ~20 V, and the measurement error should be considered, though they could also indicate that there are some small differences in the on state of the thyristors. For the 6 thyristors module shown in Fig. 5(a) the consistency of fast dropping edge becomes worse between the different thyristors, and the variation in on state voltage is larger (~40 V). We note that there are some high speed oscillations/noise on the waveforms of the trigger pulse and thyristor voltage at later times (~350 ns onwards). These are likely caused by corona discharge at the output of the spiral, which could also decrease the voltage multiplication efficiency of the spiral and limit the highest operating voltage.

B. Comparison between simulation and experimental results

The primary use for the spiral generators we are developing is to trigger high voltage Kovalchuk ball switches through distortion of the electric field between the electrodes of the switch [30]. Hence our first comparisons of the performance of the model were against such experiments, one utilizing the 6 thyristors module (i) as input switch and a charging voltage of -4.5 kV; the other using the much lower inductance 4 thyristors module (ii) as input switch and a charging voltage of -3.6 kV (the different charging voltages were used to provide comparable output voltages). The ball switch load is best described as a capacitor with a few pF in value. With the capacitance of the high voltage probe and any strays to account for, the model employed a 10 pF capacitive load. Two different versions of the model were simulated, where the switching time t_s was assumed to be zero and $0.5T_0$, respectively. Both models considered the resistive loss of the spiral generator, and a resistance R_0 = 0.42 Ω in the stripline, as calculated by (12), was employed.

Fig. 6 shows the experimental results alongside predictions from the two models. As can be seen, there is generally good agreement in both the amplitude and shape of the different voltage peaks, with differences of ~10% between simulation and experiments. Larger input switch inductance leads to lower voltage multiplication efficiency and longer oscillation period. Longer switching time results in lower 1st peak of the output voltage and slightly longer oscillation period but has little effect on the 2nd peak. After the 3rd peak the disparity between simulation and experiment starts to grow, due to changes of input switch impedance, errors caused by small differences in the inductance and capacitance of the spiral increasing with time and potentially due to the leakage current being assumed to be constant whilst it should be a function of the voltage along the stripline. It should be noted that only the first or second peak matters in most applications. This comparison demonstrates the effectiveness of the model with load of low capacitance.

Spirals utilizing the 4 thyristors input switch (module ii) had a much higher voltage multiplication efficiency (ε_{ff}=35.8%) than those with 6 thyristors, higher inductance switch (module (i), ε_{ff}=28.3%); and both results were better than early tests utilizing miniature spark gaps [30]. This indicates that the switch inductance has a significant influence on the output pulse. Switches with low inductance and fast switching speed are favorable.

C. Pulse forming process within the spiral generator

Whilst the previous section shows a good agreement between the output voltage of the model and that measured in experiment, to explain the shape of the output waveform we need to examine wave propagation along the striplines that make up the spiral. Though the propagation process was explored in Pal'chikov's simulations [23],we note there is little experimental data available for comparison. Such data is critical for validating the model's behavior – it could highlight any physical processes that need addressed in the model and might also enable improvements to a spiral generator's output.

Experimental measurements of the voltage on the active and passive layers were made using a spiral generator with monitoring tapes spaced regularly along its turns – as shown

Copyright (c) 2021 IEEE. Personal use is permitted. For any other purposes, permission must be obtained from the IEEE by emailing pubs-permissions@ieee.org.

This is the author's version of an article that has been published in this journal. Changes were made to this version by the publisher prior to publication.
The final version of record is available at http://dx.doi.org/10.1109/TPEL.2021.3063499

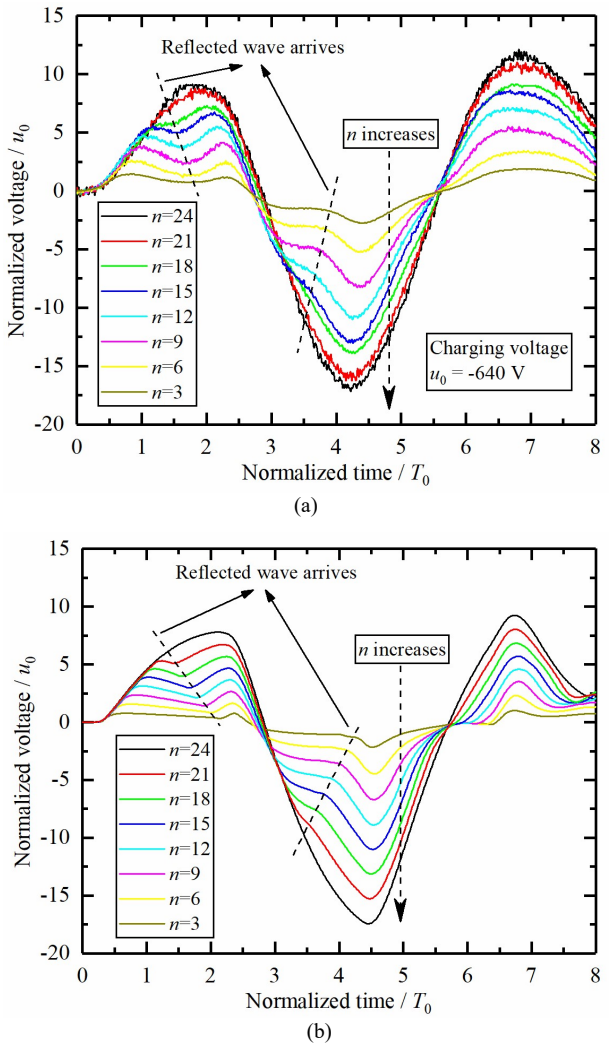


Fig. 7. Voltage on different turns of the spiral generator. (a) experimental results, where single thyristor being used as input switch; (b) simulation results, where a 10 pF capacitive load, a 10 nH switch inductance and the switching time of $0.5T_0$ being used. T_0=52.25 ns.

in Fig. 4(a). A single thyristor was used as the input switch to this generator, enabling a lower charging voltage to be employed, preventing possible breakdowns between the closely spaced tapes (if a 4 or 6 thyristors module had been employed, higher charging voltages would be needed to maintain fast switching speeds, otherwise wave reflections along the spiral could not be observed). In total the spiral had 24 turns and its output was again connected to a Kovalchuk ball switch load. In our model, to see how the voltage waveforms build on their way to the output, u_a and u_p were integrated to the same number of turns as the monitoring tapes.

Initially we studied the total voltage (the sum of active and passive contributions) throughout the spiral – the results are shown in Fig. 7, and at n=24 turns this is the output of the generator seen at ball switch. Simply exploring how this total voltage changes along the spiral's striplines immediately explains details in the shape of output voltage waveform – in particular the inflexion observed in the rising part of the first voltage pulse can be seen to build up through the different turns, and it becomes clear that this is due to the reflected wave from the open end of the stripline which arrives at different times for the various turns (marked by a dashed line in the figure).

The experimental data, however, enables comparison with the model's outputs in far greater depth - with a little processing the time-dependent distribution of both u_a and u_p along the length of the spiral can be explored. Experimental based measurements of u_a and u_p are shown in Fig. 8; whilst the output from our model are shown in Fig 9. In each figure (a)-(f) correspond to the same timings; (a)-(c) detail the voltage on the active layer, and (d)-(f) the passive; and in both figures black dashed lines have been used to indicate the changing trend of the curves. Voltage wave propagation and reflection processes can readily be observed in both figures. Both experimental data and modelling also demonstrate that u_a changes much more rapidly than that of u_p, just as the "active" and "passive" names for the layers given by Fitch and Howell [12] suggests. At this level of detail though, there are a lot of differences between experimental and simulation waveforms.

Figs. 8(a) and 9(a) show experimental measurements and simulations of the active layer as the voltage output from the spiral generator increases towards its first peak at $2T_0$. In line with the general operation principle discussed in Section IIA, the simulations show clear propagation of a discharge 'wave' from the input end of the spiral (x=0) to the far end (x=1) at a time T_0, with the potential then reversing from $-u_0$ to $+0.75u_0$, and the wave returning to the input end at $2T_0$. Once the discharge of the spiral starts, the input end remains at ~0 voltage until this reflected wave returns. The experimental results, on the other hand, show no voltage reversal during this time period at any point in the spiral. The input end of the spiral slowly increases in potential from $-u_0$ to 0, and as the discharge progresses the potential at other end of the spiral decreases to $-2u_0$ by T_0 before returning to $-u_0$ at $2T_0$. There is a standing wave structure in the measurements with a dip in potential developing at ~15 turns from the input of the spiral. Passive layer also shows differences between experimental measurements and the simulations - Figs. 8(d), and 9(d) respectively. The simulations suggest that between the initiation of the discharge and $2T_0$, the passive layer should slowly decrease in potential along its length, transitioning from $+u_0$ towards 0 by $2T_0$. Experimental results instead show that the input end of the passive layer stays relatively fixed at $+u_0$ until T_0 and only then discharges to ~0 by $2T_0$. Meanwhile, the far end of the passive layer actually increases in voltage to $\sim 2u_0$ between T_0 and $1.25T_0$ before starting to decrease. By $2T_0$ it still has a potential of $\sim 1.5u_0$.

Between $2T_0$ and $4.25T_0$, the output voltage from the spiral generator goes from the first peak, which is positive, to the second peak, which is larger in amplitude and negative. Experimental measurements of the active layer during this time are shown in Fig. 8(b), with simulations in Fig. 9(b). As expected, the simulations show the discharge of the active layer again travelling from the input end of the spiral, to the

Copyright (c) 2021 IEEE. Personal use is permitted. For any other purposes, permission must be obtained from the IEEE by emailing pubs-permissions@ieee.org.

This is the author's version of an article that has been published in this journal. Changes were made to this version by the publisher prior to publication.
The final version of record is available at http://dx.doi.org/10.1109/TPEL.2021.3063499

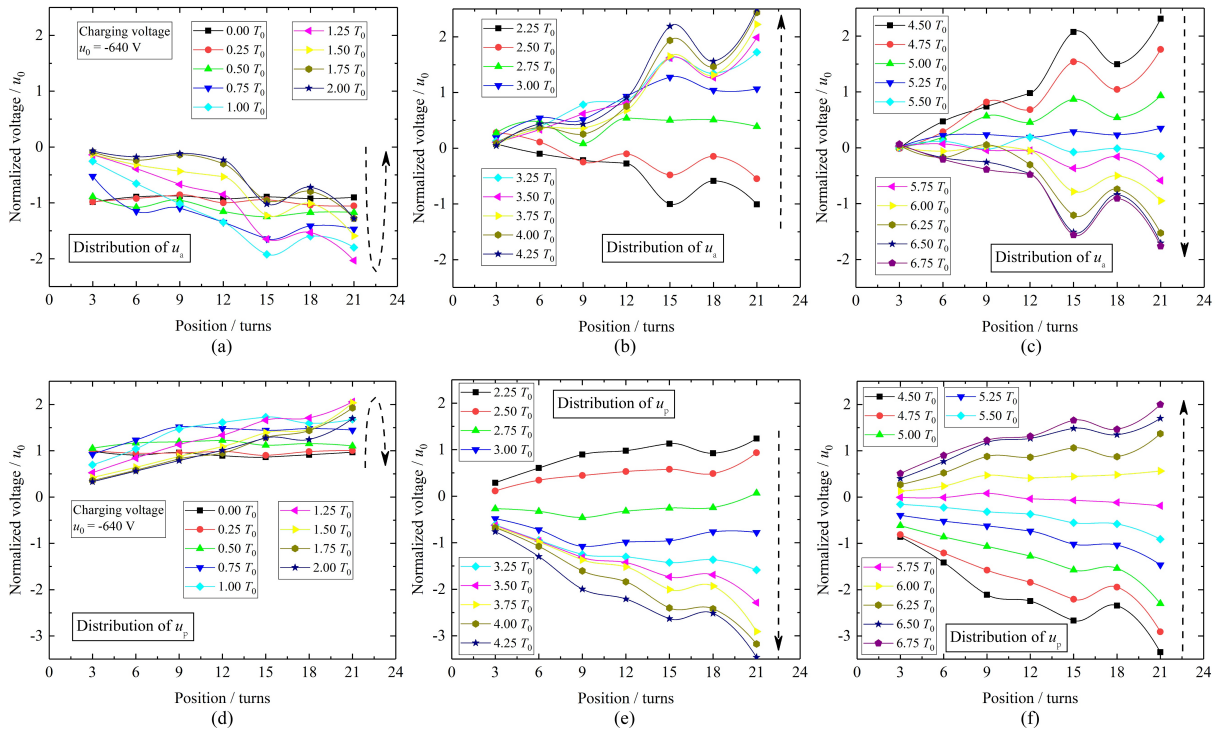


Fig. 8. Experimental results of time-resolved voltage distribution of u_a and u_p along the spiral generator. (a), (b) and (c) show the distribution of u_a; (d), (e) and (f) show the distribution of u_p. For the X-axis, turn 0 means the input terminal (x=0), and turn 24 means the output terminal (x=1). The figure corresponds to Fig. 7(a), and T_0=52.25 ns.

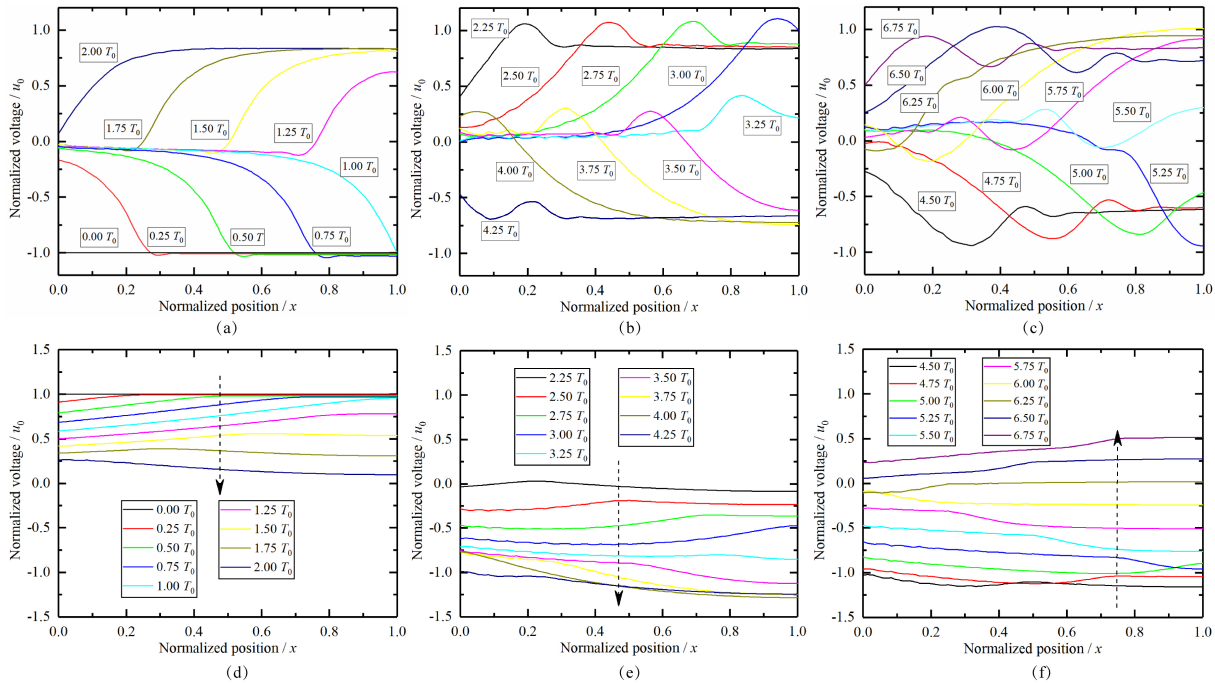


Fig. 9. Simulation results of time-resolved voltage distribution of u_a and u_p along the spiral generator. (a), (b) and (c) show the distribution of u_a; (d), (e) and (f) show the distribution of u_p. The figure corresponds to Fig. 7(b), and T_0=52.25 ns.

other end at $3T_0$, before reversing in potential and heading back to the input where it arrives at ~$4T_0$. Over the majority of this time the input end of the spiral remains at ~0 V. The discharge wave now has a clear peak in its structure and starts to elongate over the length of the spiral, by $4.25T_0$ the wave brings the majority of the active layer to a potential of -0.75u_0. Experimental measurements of the active layer show that from $2T_0$ to $4.25T_0$ the input end of the spiral does indeed remain close to zero, but there is no sudden decrease in potential associated with the arrival of any wave at ~$4T_0$. Instead the

Copyright (c) 2021 IEEE. Personal use is permitted. For any other purposes, permission must be obtained from the IEEE by emailing pubs-permissions@ieee.org.

This is the author's version of an article that has been published in this journal. Changes were made to this version by the publisher prior to publication.
The final version of record is available at http://dx.doi.org/10.1109/TPEL.2021.3063499

potential at far end of the spiral changes from -u_0 to 2.5u_0, a much larger swing in potential that predicted by the simulations. Again, there is standing wave structure in the experimental measurements, with a peak developing at ~15 turns. As before, simulations of the passive layer in Fig. 9(e) suggest a gradual discharge of the entire layer from 0 to ~-u_0 by 4.25T_0. The experimental measurements, in Fig. 8(e), show that whilst the input end of the spiral does change in potential from 0 to ~-u_0, the opposite end is significantly different, swinging from +u_0 to -3.5u_0 over this time. This huge swing in voltage along the passive layer explains why the second peak in the output from the spiral generator is so large.

Finally, we consider times between 4.25T_0 and 6.75T_0, as the output voltage from the spiral generator transitions from its negative peak, to its 3rd peak, which is positive. Simulations of the active layer, Fig. 9(c), again show the discharge travelling along the spiral from the input to the far end, reflecting at ~5.5T_0 and heading back towards the input. There is now clear structure in the discharge, a peak and small oscillation in the wave as it travels along the layer. At 6.75T_0 the layer is returned to a potential between 0.5u_0 and u_0. Experimental measurements over this time period show that the potential of the input end of the spiral remains pinned at ~0 volts. The far end of the spiral, meanwhile, swings from 2.5u_0 back to -2u_0. The peak in potential at 15 turns, now swings back into a dip. Simulation of the passive layer, as shown in Fig. 9 (f), shows that over the same time period the layer should transition from ~-u_0 volts to between 0.25u_0 and 0.5u_0. Once again, experimental measurements of the input end of the spiral do show this transition; however, opposite end of the spiral swings from -3.5u_0 back to +2u_0.

In summary, our comparisons indicate that whilst there is good agreement between experimental measurements of the output voltage of a spiral generator and our simulations, we should still treat any predictions with some caution. As Fitch and Howell indicated, there is an obvious difference between the active and passive layers in the spiral, with the active layer showing far more wave-like structures. However, in experiment, particularly towards the output end of the spiral the swings in voltage on the individual layers are larger than our simulations would predict. Further in experiments, the active layer rapidly develops a standing wave-like structure along its length. The differences between experimental results and our model could be a result of how wave propagation in the spiral connects to the load. This can be further explored by examining how the geometry of the spiral and characteristics of the load affect the output pulse.

D. Influence of inductance L_N and capacitance C_0 of the spiral

Given the principle of operation of the spiral, its inductance L_N and capacitance C_0 are expected to strongly influence the output pulse waveform - and both factors are determined by geometry. Fig. 10 shows the simulation results of different L_N and C_0. With the increase of L_N and C_0, both the amplitude of the first pulse and the oscillation period increase, while the amplitude of the second pulse decreases first and then

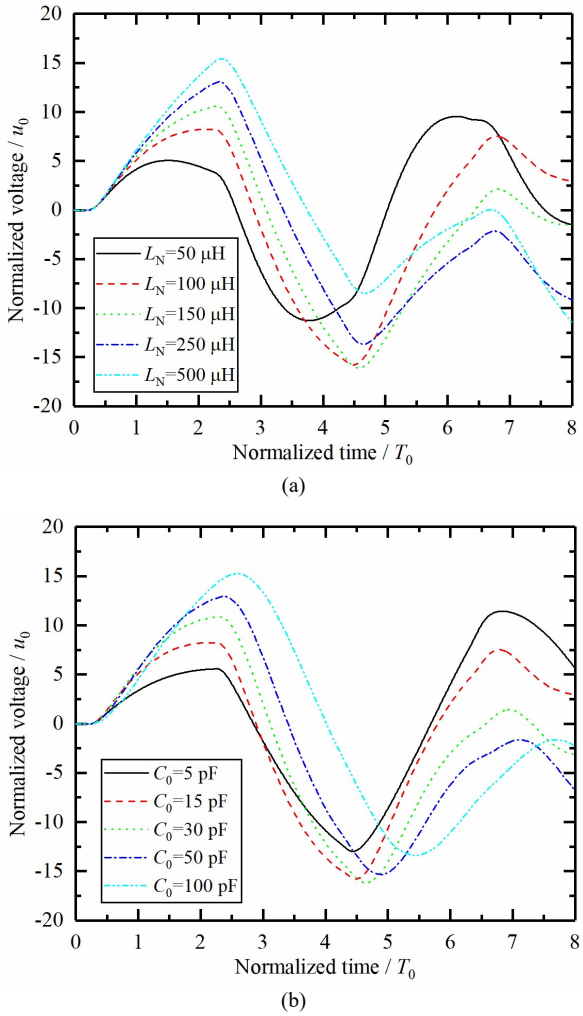


Fig. 10. Simulations of the output waveforms with different L_N and C_0. (a) effect of L_N, where C_0=20 pF and C_L=10 pF; (b) effect of C_0, where L_N=100 μH and C_L=10 pF. All the other parameters are shown in Table I.

increases. With larger L_N and C_0, the first peak can exceed the second peak.

We note, however, that although L_N and C_0 are increased by an order of magnitude in the simulations, the oscillation period does not change dramatically. This is an evidence that the wave propagation in the spiral generator dominates the duration of the pulse, and hence models that simply use lumped equivalent circuits will fail to predict the output waveforms. In fact, it is almost impossible to only adjust the value of L_N or C_0 and keep the other unchanged. For example, increasing the copper width can increase the C_0 significantly, but at the same time reduce L_N. Usually, both factors are mutually restrictive, which is one of the difficulties in designing spiral generators.

E. Geometry Scaling effects

When designing a spiral generator, it is of great importance to find the correlation between its output characteristics and geometric parameters. We investigated three different geometric parameters independently - the number of turns, N,

Copyright (c) 2021 IEEE. Personal use is permitted. For any other purposes, permission must be obtained from the IEEE by emailing pubs-permissions@ieee.org.

This is the author's version of an article that has been published in this journal. Changes were made to this version by the publisher prior to publication.
The final version of record is available at http://dx.doi.org/10.1109/TPEL.2021.3063499

the mean diameter of the winding, D, and the copper width, w - the parameters of each are shown in Table II, where L_N is the output inductance, C_{in} is the input capacitance, C_0 is the output capacitance, and l is the total length, of the spiral generator. As in Section IV.C a single thyristor input switch was again employed for these tests, with a charging voltage of 1.2 kV.

TABLE II
MEASURED INDUCTANCE AND CAPACITANCE OF SPIRAL GENERATORS WITH DIFFERENT GEOMETRIC PARAMETERS

Geometric parameters		L_N/μH	C_{in}/nF	C_0/pF	l/m
D=40 mm		18.4	6.9	6	3.02
D=80 mm	w=12 mm	57.2	14.3	12	3.03
D=120 mm	N=24	111.8	22.8	20	9.05
D=160 mm		159.0	29.4	26	12.06
w=5 mm		126.2	9.2	8	9.05
w=12 mm	D=120 mm	111.8	22.8	20	9.05
w=25 mm	N=24	93.8	43.5	38	9.05
w=50 mm		70.8	85.9	75	9.05
N=12		32.0	10.5	36	4.15
N=24	D=120 mm	111.8	22.8	20	9.05
N=36	w=12 mm	240.2	36.3	14	14.70
N=48		414.3	51.4	11	21.11

*C_{in} is measured at the input terminal, and $C_0=C_{in}/(2N^2)$.

The results are shown in Fig. 11 along with simulations made by using our model. As expected in experiments, increasing the number of turns both increased the risetime of the output voltage pulse and increased its amplitude. Whilst the same trend was seen in the simulations, the agreement between simulation and experiment became worse as the number of turns decreased, particularly for the second voltage pulse and thereafter. As the width of the copper tape was increased, experiments showed the risetime of the output voltages pulses remained similar, but the amplitude rapidly increased. Again, the simulations followed the same trend but the increase in voltage pulse was significantly lower as the tape width increased. Finally, as diameter increased, both the risetime and amplitude of the output pulse increased. Agreement with the model was good at larger diameters but became increasingly poor at the smallest diameters. We note that comparing the waveform of N=24 shown in Fig. 11(a) to that in Fig. 6, a higher voltage multiplication efficiency was obtained in the experiment due to the even smaller switch inductance and faster switching speed.

The comparisons between experiments and simulations indicate the limitations of the model. Generally, the model performs better in cases of a large number of turns, thin copper tape, and a large mean diameter – i.e. all cases when wave propagation becomes more important. Several assumptions and simplifications in our model could lead to the inaccuracies that are seen between the experiment and the simulations. Firstly, the equivalent capacitance of the spiral generator only exists during the transition of the pulse forming process, and the energy is then distributed and stored along the stripline; thus, the lumped assumption we use when considering how the spiral connects to the input switch and load will lose validity in some cases. Secondly, energy consumed by the load should be inductively transferred by the magnetic field instead of the leakage current. What's more, the leakage current should be determined by wave voltage along the stripline instead of being constant. Considering all these

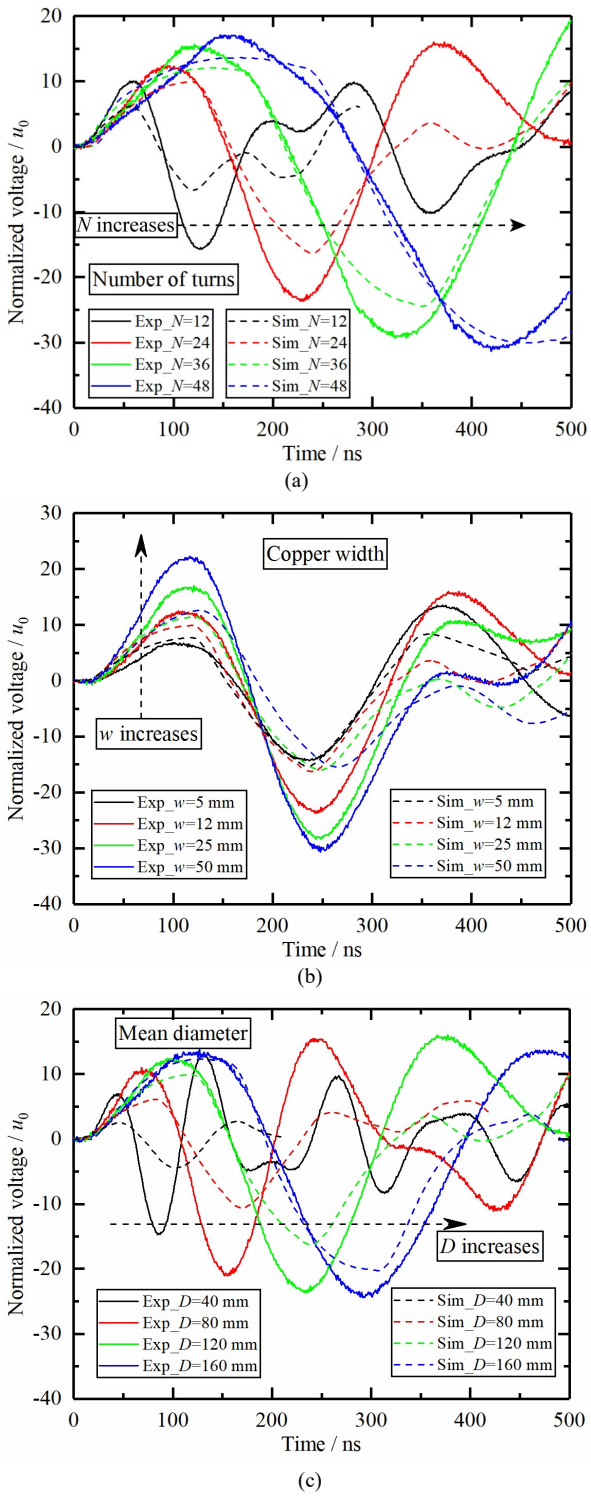


Fig. 11. Dependency of output waveforms with different geometric parameters. (a) effect of number of turns, where the inner diameter of the winding remains 100 mm; (b) effect of copper width; (c) effect of mean diameter of the winding, where the thickness of the winding remains 20 mm. A single thyristor is used as input switch, and the charging voltage is -1.2 kV. All the other parameters are shown in Table I.

Copyright (c) 2021 IEEE. Personal use is permitted. For any other purposes, permission must be obtained from the IEEE by emailing pubs-permissions@ieee.org.

This is the author's version of an article that has been published in this journal. Changes were made to this version by the publisher prior to publication.
The final version of record is available at http://dx.doi.org/10.1109/TPEL.2021.3063499

factors, predictions from the model are very precise in cases where wave process is dominant (relative error < 10%) while only qualitatively in line with the changing trend when considering scaling and loading effects.

F. Load effects

Resistive, capacitive and inductive loads were tested, again using a single thyristor input switch. The experiment results are shown in Fig. 12. Simulation results are not presented here due to the large number of waveforms; as with the results of the previous section, the simulations show the same trends as the experimental results but the relative errors in amplitude and oscillation period can become very large in some cases.

For a resistive load, when resistance is larger than 50 kΩ, the output pulse remains unchanged. When decreasing the load resistance, only the amplitudes of the peaks are reduced, while the oscillation period remains unchanged. For a capacitive load, the oscillation period increases, and the amplitude decreases as the load capacitance increases. For an inductive load, a multi-turn winding with a Ferrite core was used to produce the large inductances, and two wires with different lengths ($l_{II} > l_I$) were employed. Due to its longer length, wire II leads to longer oscillation periods than Wire I. This might be caused by the saturation of the magnetic core during the discharge which changes the inductance.

G. Output pulses for various applications

Based on the thorough investigations presented above, several different kinds of spiral generators were built for some potential applications - driving a high voltage Dielectric Barrier Discharge (DBD), triggering a new type of High Current Solid State switch and triggering a Kovalchuk Ball switch through field distortion. Each required different output characteristics.

Fig 13(a) shows the results from a 24 turns, 40 mm diameter spiral with 12 mm wide tape that could be used to drive a DBD. With a charging voltage of only ~800V, short duration 10 kV amplitude pulses were produced with a repetition rate of 10 kHz. The amplitude could be further adjusted by simply changing the charging voltage, and the repetition rate was limited mainly by the available power supply used to charge the spiral.

Pulses in Fig. 13(b) have a very fast rising edge produced by connecting the output of a 24 turns, 120 mm diameter spiral to a pulsed sharpening gap. This is intended to trigger a new type of high current solid state switch that requires extremely high rates of voltage rise (2-3 kV/ns). The load here is about 110 pF, hence the width of the copper tape in the spiral was increased to ~50 mm to counteract the reduced output voltage. Two kinds of pulse sharpening gaps were employed: commercial vacuum gaps with the rated voltage of 5 kV, and self-made polarity dependent gap in dry air. The voltage rising rates are 0.60 kV/ns, 0.83 kV/ns, 1.03 kV/ns, 0.98 kV/ns, and 9.98 kV/ns, respectively.

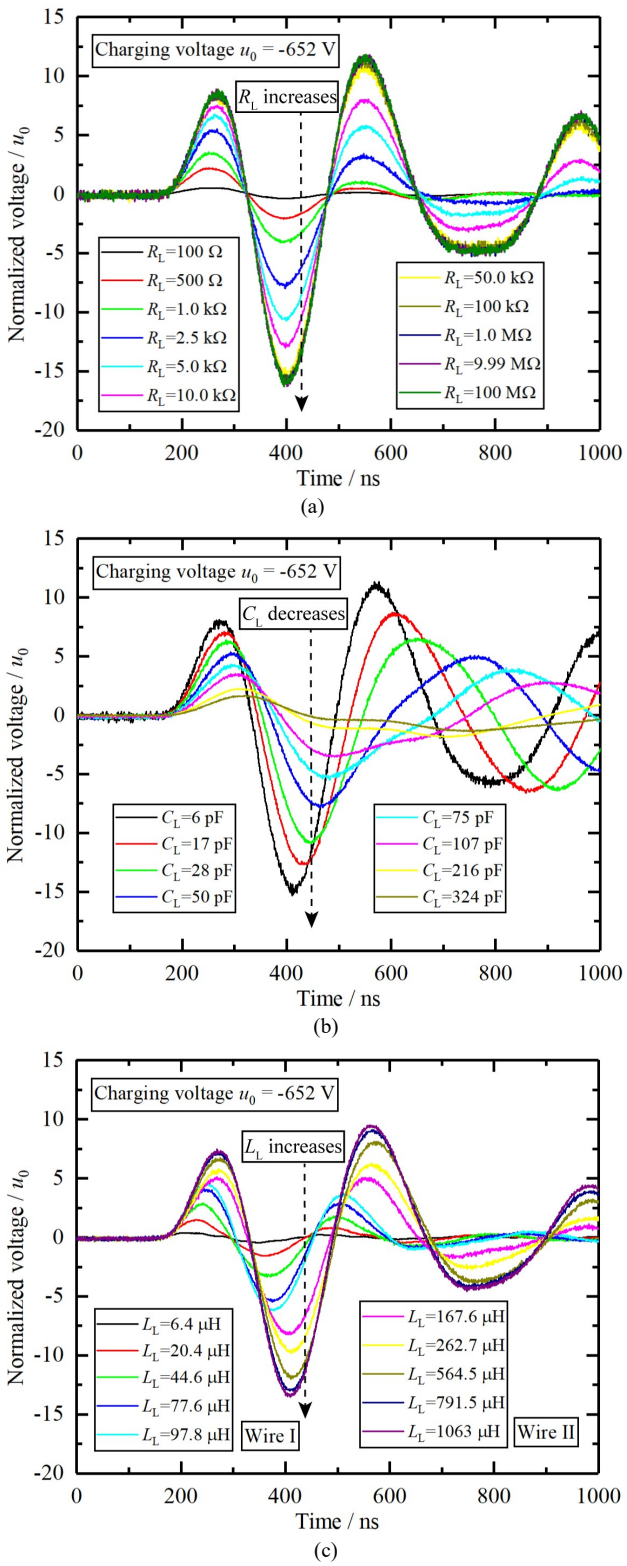


Fig. 12. Dependency of output waveforms with different types of load. (a) the resistive load; (b) the capacitive load; (c) the inductive load. Single thyristor is used as the input switch.

Pulses shown in Fig. 13(c) were produced by a 24 turns, 120 mm diameter spiral with 12 mm wide tape and are

Copyright (c) 2021 IEEE. Personal use is permitted. For any other purposes, permission must be obtained from the IEEE by emailing pubs-permissions@ieee.org.

This is the author's version of an article that has been published in this journal. Changes were made to this version by the publisher prior to publication.
The final version of record is available at http://dx.doi.org/10.1109/TPEL.2021.3063499

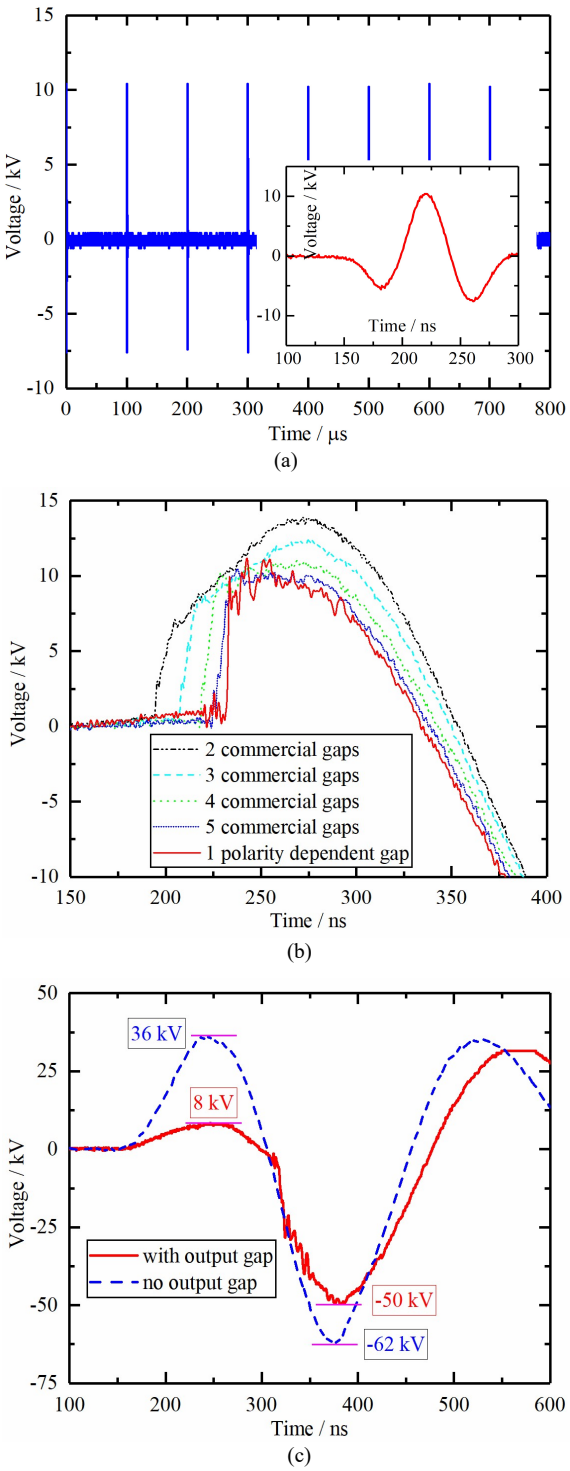


Fig. 13. Pulses for different applications. (a) single thyristor as the input switch, the charging voltage is +800 V, the repetition rate is 10 kHz, and the load is 5 pF; (b) single thyristor as the input switch, the charging voltage is -1.2 kV, the load is 110 pF, and several different output sharpening gaps are used; (c) module (ii) as the input switch, the charging voltage is -3.6 kV, the load is 10 pF, and the polarity dependent sharpening gap is used.

intended to trigger a Kovalchuk Ball gap used in large pulsed power systems. To make full use of the feature that the second peak is much higher than the first peak of the output pulse, a polarity dependent gap is used to suppress the first peak and sharpen the second peak. The amplitude is about -50 kV, and the rising time is about 50 ns. The details are presented in another paper [30]. The entire spiral generator along with control and charging electronics can be fitted into a case 210×145×33 mm. As can be seen, with minor improvements, spiral generators can be used in a variety of situations and have the characteristics of high voltage multiplication efficiency, fewer components, and compact structure.

V. Conclusion

In this paper, the detailed experimental and simulation results of the spiral generator are presented. In experiments, two kinds of series-connected thyristor modules and a single thyristor were used as the input switches which enable low trigger jitter, high repetition rate and long lifetimes. Good consistency of the static voltage balance and switching process of the series-connected thyristors was observed. A special spiral generator with multiple monitoring points spaced along its length was also built to investigate the voltage wave propagation. A model was developed in which the voltage multiplication process is divided into two aspects - wave propagation along the stripline described by Telegraph equations and the charge exchange described by the equivalent circuit formed by the inductance and capacitance of the spiral. A good fit between experimental and simulation results verified the reliability of the model as long as the wave propagation dominates the circuit.

The experimental fact that the first peak of the output voltage pulse is often observed to be lower than subsequent peak(s) is found to be determined by the wave propagation along the spiral generator, and the peaks correspond to the conditions that the reflected waves on ‘passive’ and ‘active’ layers of the spiral reach a maximum. The voltage wave on the active layer changes more dramatically than that on the passive layer. The layer voltage can be three times larger than charging voltage, which should be considered when deciding on the thickness of the layer insulation.

Lower switch inductance and short switching times are beneficial to reduce the oscillation period and increase the output voltage. Geometric parameters (mean diameter, number of turns and width of the copper tape) influence the oscillation period and the voltage multiplication efficiency by changing the wave propagation time and the inductance and capacitance of the spiral. The parameter combinations, such as larger mean diameter and copper width, that can increase the equivalent impedance and output capacitance of the spiral are beneficial to increase the voltage multiplication efficiency ε_{eff}. Though larger number of turns can increase the output voltage, it usually results in lower ε_{eff}. With larger L_N and C_0, the first peak can even exceed the second peak. A resistive load only changes the amplitudes of the output pulses, whilst capacitive and inductive loads influence both the period and amplitude.

Three kinds of applications of the spiral generator are presented - pulses with 10 kV amplitude and 10 kHz repetition rate for driving DBD plasma; pulses with amplitude of 10 kV and 10 kV/ns rising rate for driving new high current solid

Copyright (c) 2021 IEEE. Personal use is permitted. For any other purposes, permission must be obtained from the IEEE by emailing pubs-permissions@ieee.org.

This is the author's version of an article that has been published in this journal. Changes were made to this version by the publisher prior to publication.
The final version of record is available at http://dx.doi.org/10.1109/TPEL.2021.3063499

state switches of high input capacitance; and pulses with -50 kV amplitude and 50 ns rising time for triggering high power gas switches through field distortion.

This research has been carried out as part of the 'Brick 2' project at Imperial College that aims to make the next generation of pulsed power brick incorporating on board high voltage charging, triggering and safety systems; creating a user friendly building block for new pulsed power generators. The brick will be simple to build and easy to adapt for different capabilities.

ACKNOWLEDGMENT

The authors would like to express our thanks and appreciates to Yakov Krasik of Technion, Bucur Novac and Peter Senior of Loughborough University, John Waldron of Silicon Power Corporation, Savva Theocharous and Jergus Strucka of Imperial College London.

REFERENCES

[1] D. Z. Pai *et al.*, "Nanosecond repetitively pulsed discharges in air at atmospheric pressure-the glow regime," *Plasma Sources Sci. Technol.*, vol. 18, no. 4, October 2009, Art. no. 045030.

[2] S. Shen *et al*., "Further Investigations on a Modified Avalanche Transistor-based Marx Bank Circuit," *IEEE Trans. Instrum. Meas.*, May 2020.

[3] A. A. Elserougi, A. M. Massoud and S. A. Ahmed, "Modular high-voltage pulse-generator with sequential charging for water treatment applications," *IEEE Transactions on Industrial Electronics*, vol. 63, no. 12, pp. 7898-7907, January 2016.

[4] J. Yan *et al.*, "A novel trigger for pseudospark switch with high repetition rate, low jitter, and compact structure," *Rev. Sci. Instrum.*, vol. 89, no. 6, June 2018, Art. no. 065102.

[5] I. V. Lavrinovich *et al*., "A compact pulsed X-ray source for high-speed radiography," *Instruments and Experimental Techniques*, vol. 56, no. 3, pp. 329-334, June 2013.

[6] I. Adamovich *et al*., "The 2017 Plasma Roadmap: Low temperature plasma science and technology," *J. Phys. D: Appl. Phys.*, vol. 50, no. 32, July 2017, Art. no. 323001.

[7] L. Pang *et al*., "A compact series-connected SiC MOSFETs module and its application in high voltage nanosecond pulse generator," *IEEE Trans. Ind. Electron.*, vol. 66, no. 12, pp. 9238-9247, January 2019.

[8] J. Yan, S. Shen and W. Ding, "High-Power Nanosecond Pulse Generators with Improved Reliability by Adopting Auxiliary Triggering Topology," *IEEE Trans. Power Electron.*, vol. 35, no. 2, pp. 1353-1364, June 2019.

[9] D. Zhang *et al*., "A compact, high repetition-rate, nanosecond pulse generator based on magnetic pulse compression system," *IEEE Trans. Dielectr. Electr. Insul.*, vol. 18, no. 4, pp. 1151-1157, August 2011.

[10] L. Zhao *et al*., "A Tesla-type repetitive nanosecond pulse generator for solid dielectric breakdown research," *Rev. Sci. Instrum.*, vol. 84, no. 10, October 2013, Art. no. 105114.

[11] W. Jiang, "Review of solid-state linear transformer driver technology," *Matter and Radiation at Extremes*, vol. 3, no. 4, pp. 159-164, December 2018.

[12] R. A. Fitch and V. T. S. Howell, "Novel principle of transient high-voltage generation," *in Proc. of the Institution of Electrical Engineers.* vol. 111, no. 4, pp. 849-855, April 1964.

[13] For instance, the PT55 generator produced by Pacific Atlantic Electronics (now closed) http://paeinc.us/pt-55.htm, accessed 30th Nov 2020.

[14] S. A. Merryman, M. F. Rose and Z. Shotts, "Characterization and applications of vector inversion generators," *in Proc. 14th IEEE International Pulsed Power Conf.*, vol. 1, pp. 249-252, June 2003.

[15] M. F. Rose, Z. Shotts and Z. Roberts, "High efficiency compact high voltage vector inversion generators," *in Proc. 15th IEEE Pulsed Power Conf.*, pp. 1207-1210, June 2005.

[16] J. Hanlon *et al*., "High voltage solid state switched Vector Inversion Generators," *in Proc. 16th IEEE International Pulsed Power Conf.*, vol. 1, pp. 918-922, June 2007.

[17] Z. Shotts, Roberts and M. F. Rose, "Design principles for vector inversion generators," *in Proc. 16th IEEE International Pulsed Power Conf.*, vol. 1, pp. 556-559, June 2007.

[18] Z. Shotts, Roberts and M. F. Rose, "Limits and failure modes in high voltage Vector Inversion Generators," *in Proc. 17th IEEE International Pulsed Power Conf.*, vol. 1, pp. 902-907, June 2009.

[19] S. I. Shkuratov *et al*., "Completely explosive autonomous high-voltage pulsed-power system based on shockwave ferromagnetic primary power source and spiral vector inversion generator," *IEEE Trans. Plasma Sci.*, vol. 34, no. 5, pp. 1866-1872, October 2006.

[20] S. I. Shkuratov *et al*., "Completely explosive ultracompact high-voltage nanosecond pulse-generating system," *Rev. Sci. Instrum.*, vol. 77, no. 4, April 2006, Art. no. 043904.

[21] D. Sheftman *et al*., "Diagnostics of underwater electrical wire explosion through a time-and space-resolved hard x-ray source," *Rev. Sci. Instrum.*, vol. 83, no. 10, October 2012, Art. no. 103505.

[22] E. I. Pal'chikov *et al*., "Pulse X-ray Device Based on a Combined Spiral Generator," *Journal of Applied Mechanics and Technical Physics*, vol. 60, no. 3, pp. 586-591, August 2019.

[23] E. I. Pal'chikov, A. M. Ryabchun and I. Y. Krasnikov, "Modified spiral high-voltage generator for feeding a pulsed X-ray apparatus," *Technical Physics*, vol. 57, no. 2, pp. 292-301, February 2012.

[24] F. Rühl and G. Herziger, "Analysis of the spiral generator," *Rev. Sci. Instrum.*, vol. 51, no. 11, pp. 1541-1547, June 1980.

[25] "Increasing the Pulse Repetition Rate for Solid State Thyratron Replacements", contributed talk by J., Waldron, IEEE PPPS conference, Orlando, Florida 2019. Abstract can be found at: https://indico.cern.ch/event/727938/timetable/?print=1&view=standard (accessed 1st December 2020)

[26] J. Waldron, K. Brandmier and V. Temple. "Ultra-fast, high reliability solid state thyratron, ignitron and thyristor replacement," *in Proc. IEEE International Pulsed Power Conf.*, 1-5, June 2015.

[27] J. Waldron and K. Brandmier. "Second Generation High-Voltage, Ultra-Fast, High Reliability Solid State Thyratron Replacements," *in Proc. IEEE International Conf. on Plasma Sci.,* 1-1, June 2017.

[28] E. I. Bichenkov, *et al*., "On the refinement of the theoretical model for a high-voltage spiral generator," *Technical Physics*, vol. 52, no. 12, pp. 1597-1603, December 2007.

[29] F. W. Grover, "Tables for the calculation of the inductance of circular coils of rectangular cross section," *US Government Printing Office*, 1922.

[30] J. Yan et al., "A miniature solid-state switched spiral generator for cost effective, programable triggering of large scale pulsed power accelerators," *Phys. Rev. Accel. Beams*, February 2020 (accepted).

Copyright (c) 2021 IEEE. Personal use is permitted. For any other purposes, permission must be obtained from the IEEE by emailing pubs-permissions@ieee.org.